HHS Public Access

Author manuscript

IEEE Int Conf Robot Autom. Author manuscript; available in PMC 2022 October 18.

Published in final edited form as:

IEEE Int Conf Robot Autom. 2021 ; 2021: . doi:10.1109/icra48506.2021.9561685.

A Confidence-Based Supervised-Autonomous Control Strategy for Robotic Vaginal Cuff Closure

Michael Kam[1], **Hamed Saeidi**[1], **Michael H. Hsieh**[2], **J. U. Kang**[3], **Axel Krieger**[1] **[Member, IEEE]**

[1]Dep. of Mechanical Engineering, Johns Hopkins University, Baltimore, MD 21211, USA

[2]Dep. of Urology, Children's National Hospital, 111 Michigan Ave. N.W., Washington, DC 20010, USA

[3]Dep. of Electrical and Computer Engineering, Johns Hopkins University, Baltimore, MD 21211, USA

Abstract

Autonomous robotic suturing has the potential to improve surgery outcomes by leveraging accuracy, repeatability, and consistency compared to manual operations. However, achieving full autonomy in complex surgical environments is not practical and human supervision is required to guarantee safety. In this paper, we develop a confidence-based supervised autonomous suturing method to perform robotic suturing tasks via both Smart Tissue Autonomous Robot (STAR) and surgeon collaboratively with the highest possible degree of autonomy. Via the proposed method, STAR performs autonomous suturing when highly confident and otherwise asks the operator for possible assistance in suture positioning adjustments. We evaluate the accuracy of our proposed control method via robotic suturing tests on synthetic vaginal cuff tissues and compare them to the results of vaginal cuff closures performed by an experienced surgeon. Our test results indicate that by using the proposed confidence-based method, STAR can predict the success of pure autonomous suture placement with an accuracy of 94.74%. Moreover, via an additional 25% human intervention, STAR can achieve a 98.1% suture placement accuracy compared to an 85.4% accuracy of completely autonomous robotic suturing. Finally, our experiment results indicate that STAR using the proposed method achieves 1.6 times better consistency in suture spacing and 1.8 times better consistency in suture bite sizes than the manual results.

I. INTRODUCTION

Robot-Assisted Minimally Invasive Surgery (RAMIS) systems take advantage of highly dexterous tools, hand tremor motion filtering and scaling to improve patient outcomes by reducing patient recovery times and collateral damage [1]. However, majority of state of the art systems for robotic assisted surgeries are based on a tele-operated paradigm. As an example, the pioneer and commercially successful da Vinci Surgical System (Intuitive Surgical, Sunnyvale, California) [2] has been utilized in a wide range of surgical procedures in urology, cardiothoracic, and general surgery. Raven surgical robot developed at the

mkam2@jhu.edu .

University of Washington [3] and Senhance system from TransEnterix (Morrisville, NC) are other examples of tele-operated systems.

Autonomous control algorithms for RAMIS benefit from robotic accuracy and repeatability during surgical procedures. Such systems possess the potential to reduce human errors, deliver improved patient outcomes independent of surgeon's training and experience, and also allow remote surgeries without high-bandwidth networks [4]. Pre-planned autonomous RAMIS was implemented in bony orthopedic procedures (e.g. ROBODOC, Caspar, and CRIGOS), radiotherapy, and cochlear implants [5], [6]. Efforts in automating deformable and unstructured soft tissue surgeries include knot tying, needle insertion, deformable tissue tracking, and executing predefined motions [7]–[12]. Machine learning techniques were introduced in robotic suturing to facilitate system calibration [13] and to imitate surgical suturing from video demonstrations [14].

However, achieving full autonomy in complex surgical environments is not infallible and surgeon supervision and control take over is critical for safe operation. Our goal is to develop a supervised-autonomous control strategy that enables performing complex surgical procedures via both autonomous robot and surgeon collaboratively with the highest *possible* degree of autonomy, while ensuring safe operations. Thus a critical element in achieving this objective effectively is designing algorithms that will make the autonomous robot "self-aware" of the limitations of its automation capabilities. Such algorithms innovate by *maximizing the level of automation* of the RAMIS and *minimizing the expected errors of the variables* for which the robot is confident of performing more accurately than its human supervisor via an effective collaboration between the two.

Collaborative control strategies take the general form

$$U(t) = \alpha(t)M(t) + (1 - \alpha(t))A(t), \tag{1}$$

where $M(t)$ are the manual control commands from a human operator that are combined with the autonomous control commands $A(t)$ via complementary scales $\alpha(t) \in [0, 1]$ and $1-\alpha(t)$ respectively in order to control the robot via the total control input $U(t)$. Typical examples of such control inputs include position and velocity profiles, and force/torque.

Based on the application, different methods have been proposed for defining the function $\alpha(t)$. The goal is to determine $\alpha(t)$ dynamically based on an independent variable while the robotic control task is on the fly to fulfill certain performance criteria. Some examples include, dynamically changing $\alpha(t)$ based on position tracking accuracy [15], proximity to obstacles and/or desired locations [16], the prediction of human intentions in controlling the robot [17], and the trust of human to the autonomous controller of robot [18]. In surgical applications, the robot autonomously constrains the roll-pitch-yaw motion of the surgical tool for precision drilling by the surgeon [19] or for avoiding collisions, joint limits, and singularities [20]. Shared autonomy has also been proven effective for reducing the complexity of steering flexible robotic endoscopes [21] and flexible surgical manipulators [22]. Such techniques have been utilized for improving the tissue cutting precision of surgical robots [23].

In our previous work we developed and examined a confidence-based shared control strategy for our Smart Tissue Autonomous Robot (STAR) with applications in electrosurgery [23]. In this work, we extend the "self-aware" confidence-based strategies to robotic suturing with an application in vaginal cuff closure via the tesbed shown in Fig. 1. This requires the design and development of new methods for a discrete-time human intervention in a supervised autonomous strategy which can be extended to similar surgical tasks. In our proposed method, the robotic system generates a suture plan and continuously tracks tissue deformations as common disturbances during surgery to update the produced plan. However, the system dynamically assesses the confidence levels in completing each step of the suturing process autonomously (based on tissue deformation) and suggests to the operators to intervene and fine-tune a suture point location if it is not feasible for the robot to complete that specific suture purely autonomous. Compared to our previous work [24], the new method takes advantage of human supervision to reduce the chance of sporadic autonomous control mistakes specially when the robot has to complete a long task in pure autonomous mode. This method can also provide an easier path towards regulatory approvals for the resulting RAMIS.

In summary, the contributions and novelty of the paper include: i) developing a confidence-based supervised control strategy for robotic suturing tasks, ii) assessing the performances of the autonomous control resource and identifying the confidence models for robot as well as the confidence-based allocation function $\alpha(t)$, and iii) experimentally evaluating the accuracy of our proposed control strategy via multiple tests on synthetic vaginal cuff models and comparing them with pure manual vaginal cuff closures. The first contribution allows the human operator to intervene in the control system from a higher level (i.e. sporadic command adjustments instead of continuously sharing the control with the robot), which is different than the method in [23]. Moreover, the confidence model novelties focus on a different surgical task which include different inputs and performance criteria and decision-making processes. Our proposed shared control strategy is depicted in Fig. 2. The remainder of this paper is organized as follows. The robotic system and the planning and control methods are detailed in Section II. The results of tests via the proposed method are presented in Section III and discussed in Section IV. Section V concludes the paper.

II. Method

A. Experiment Setup

The experiment setup for our STAR system is shown in Fig. 1.a. A 7-DOF KUKA LBR Med lightweight arm (KUKA AG, Augsburg Germany) and an actuated suturing tool based on commercial Endo360° suturing device from EndoEvolution (North Chelmsford, MA, USA) were used to perform the suturing tasks. The tool was modified by adding two DC brush motors (Maxon Motors, Sachseln, Switzerland) to drive a circular needle and control a pitch rotation of the tool tip [25]. EPOS2 controllers (Maxon Motors, Sachseln, Switzerland) were used for precise positioning control, and were connected into a host computer using a controller area network (CAN). An multi-axis force sensor (ATI industrial automation, NC, USA) was used to measure the tensioning force to prevent tissue from damage during suturing tasks.

The dual camera imaging system (Fig. 1.b.) consists of a RGBD camera, Realsense D435 (Intel Corp., Santa Clara, California), and 845nm±55nm 2D NIR camera (Basler Inc., Exton, PA). The 3D camera detects 3D tissue surface information and the 2D Near-infrared (NIR) camera detects the location of NIR markers. In the study, a light source with 760 nm light-emitting diode (North Coast Technical Inc., Chesterland, OH) was used to excite the fluorophore, enabling the NIR markers to be visualized with the NIR camera, shown in Fig. 1.c. The coordinate system of the 2D NIR image was registered to that of 3D camera through camera calibration. The 3D position of the NIR markers can be found by ray tracing the NIR marker positions via a coregistered point cloud from the 3D camera, shown with color points in Fig. 1.d. A hand-eye calibration registered the 3D camera coordinate system onto the robot coordinate system by using a calibration rod and a checkerboard [26]. The 3D location of the markers w.r.t. robot frame were obtained and used by STAR for suturing tasks.

In our previous studies [27], the Near-infrared florescent (NIRF) marking technique plays a key role to enable our 3D vision tracking system to successfully track markers location. NIR markers have high signal to noise ratio (SNR) and strong signal penetration to improve target detection from background even under obstruction of blood and tissue, and therefore are suitable for intra-operative robot guidance [28]. The spatial locations of NIR markers are extracted by a dual camera system and can be utilized for vision-guidance tasks.

B. Surgical Task and Evaluation Criteria

In this paper, we utilize STAR to perform vaginal cuff closure on synthetic vaginal cuff tissue (3-Dmed, Ohio, United States). Synthetic tissue, with 5 cm diameter and 5 mm wall thickness, was chosen since it is designed for surgical training in vaginal cuff closure. The test samples were fastened within a 3D printed ring with two stay sutures coming from the side and two alligator clips clamping sample's edge from the bottom to simulate the clinical scenario including the attachment of the vaginal cuff to surrounding tissue [24]. The test sample with the 3D printed ring was placed in front of the dual camera system with distance of 35-38 cm which satisfies the minimum sensing distance of the camera. NIR markers were used manually placed on the cross section edge of the tissue prior to the suturing task only performed by STAR. The suturing results performed by STAR were compared to manual results of our previous study [24] on i) total time to complete, ii) suture spacing (i.e. the distance between consecutive stitches), and iii) bite size (i.e. distance from where a stitch enters into tissue to the tissue surface). The latter two measures are relevant to post surgical complications such as infection and dehiscence [29]. Statistic analysis including T-test and Levene's test were utilized to compare averages and variances, respectively, for the evaluation criteria. Furthermore, to compare the new confidence-based method with pure autonomous control, we compared the number of hit and misses (correct/incorrect suture placements) and the percentage of human intervention.

C. Control System

Fig. 3 shows the block diagram of the autonomous controller with occasional confidence-based human interventions for fine adjustments on the tool position. In the control loop, finding the 3D position of the NIR markers via the dual-camera system was explained earlier

in Secion II-A. A suture planner utilizes the NIR markers and the point cloud to determine the desired location of each knot and running stitch. The suture planner incorporates a planning method developed in our previous work [24] consisting of a point cloud path planning method to initialize a suture plan based on the NIR marker positions followed by a non-rigid registration method for updating a new suture plan on a deformed tissue during the suturing steps. The details of the path planning method can be found in [24] and are not discussed here since they are not the focus of this paper.

The confidence based allocation subsystem, via the method detailed in Section II-D which is the main focus of the paper, will determine which sutures from the suture planner can be done autonomously and which ones will require a possible human intervention. In the GUI (shown in Fig. 2), autonomous suture points are highlighted in green and manually adjusted points highlighted in red. The user modifies the suture point location via slider bars in 3 dimensions if the initial semi-autonomous suture placement attempt for the red points results in a misplaced suture. Thus, operator supervises the robot when manual mode with $\alpha = 1$ is selected (also referred to as assisted mode here) and only modifies the target suture point location if needed.

Finally, a high-level suturing logic and task planner then receives the resulting 3D coordinates of the suture points in the robot frame and plans the sequence of robot motions to complete the knot and running stitches on the desired and equally spaced positions [30]. This includes a combination of approaching the tissue, biting (firing the needle), tensioning, and releasing the suture. For completing knots, the process of approaching and biting the tissue is executed twice in the same place to form a tie and lock the knot into place. For completing the running stitches, STAR only executes one round of approaching the tissue, biting, tensioning, and releasing. For each suture, the high-level task planner will stop tensioning once a maximum tension force of 2 N or a tension distance of 20 cm (dropping by 5mm after each stitch) was reached without tearing the tissue.

D. Confidence Level Evaluation

In this section, we explain the process of initial data collection for confidence level evaluation and model fitting. A variation of this process determining which sutures can be performed autonomously and which possibly require human intervention is implemented and detailed later in Section III.

The main factor affecting the correct suture placement that we discovered in our prior study [24] is whether the location of a new suture point was accurately estimated on an actual tissue for a robot to successfully reach. Fig. 4.a shows an example of a planning scene with new suture points updated by the planner. The suture point in Fig. 4.b is placed on the inside edge of the vaginal cuff, which indicates a lower chance for the needle to successfully catch the tissue. The suture point shown in Fig. 4.c, has a higher chance for a stitch to be placed successfully since its location is in middle from both side of the tissue. The suture point placed on empty area in Fig. 4.d has no chance for the robot to complete a stitch since no physical target is present at the target location.

In addition to how accurately the suture point is estimated by the planner, the geometry of the suture tool also affects the chance of successfully reaching the target. If the tissue portion appears more in the needle jaw as the suturing tool approaches the target, as shown in Fig. 4.e, the suture tool has a higher chance to catch the target, and vice versa (Fig. 4.f). Our hypothesis is that the robot confidence for placing a stitch successfully on a suture point is associated with tissue information near the suture point, and the geometrical information of the tool-tip projected at the suture point. After collecting this information, an identification process will be carried out to determine a confidence model. In the real-time experiments, the resulting model will be used to evaluate the confidence level for success in completing a stitch on a suture point and hence autonomy allocation. Next, we explain the data collection process for the model identification.

Data Collection: In the data collection step, we collect the point cloud near a target location within a region based on the geometrical information of the suture tool-tip. A vaginal cuff phantom tissue is used as a target and is placed in the dual camera view (Fig. 4.g). We first command the robot to reach a target location which is manually selected from the RGBD camera view through a software interface. We define a rectangular box, shown in green in Fig. 4.g, with the same dimensions ($10mm \times 3mm \times 8mm$) of the needle jaw and collect point cloud within the box using a passthrough filter in Point Cloud Library (PCL) [31]. The orientation of the box is assigned with an identical orientation of the actual tool-tip w.r.t. the robot base frame. The collected point cloud in the box are categorized into two groups (Fig. 4.h): points in jaw (PIJ), shown as green points, and points on tool (POT), shown as red points. PIJ are points that are projected to be within the tool jaw if the tool moves exactly to the suture position, whereas POT are the counterpart points that are projected to collide with the tool jaw. The boxes are used to collect the PIJ and POT on the selected locations, shown in Fig. 4.i. An additional information of whether the robot hits or misses (HM) is recorded by commanding the robot to reach each target location and visually examining whether the needle penetrates the target. The data is evaluated through MATLAB (MathWorks, Natick, MA, USA) to find a confidence model.

III. Results

A. Data Collection for Identification of Confidence Models

Fig. 5.a shows the result of the data collection process. A total of 94 data points were collected by using the methods described in section II-D. Each data point encapsulates three sets of information: PIJ, POT, and HM. Notice that the resolution of point cloud in an area can be affected by how far the target is placed away from the RGBD camera. In this study, the target tissue was located within a 35-38 cm distance from the RGBD camera which satisfies minimum sensing distance of the camera as well as sufficient workspace for the robot to operate. In Fig. 5.a, both axes were cut off at 20 since there are no more than 20 points observed in each categories under chosen camera distance. The HM data is plotted with 0 representing a miss and 1 representing a hit. Examples of individual data points are shown in the in Fig. 5.a. Fig. 5.a.I shows data points with low PIJ which indicate low chances for robot to place suture in the correct location. Data points with high PIJ and high POT, as shown in Fig. 5.a.II, result in a similar number of hit and miss because the data

could be on a flat surface (resulting in a miss) or a narrow opening on the tissue which is not detected by the camera but it's feasible for the robot to reach (resulting in a hit). Data points with high PIJ but low POT, shown in Fig. 5.a.III, contain more successful targeting cases (i.e. HM = 1). With most PIJ estimated in the jaw only, a tool-tip has a higher chance to fit the target inside the jaw and avoid tool collision. Lastly, data points with extremely low PIJ and low POT in Fig. 5.a.IV mostly indicate the robot will fail to reach the target (i.e. HM = 0), since there is no point cloud presented in the scene.

B. Selection of Confidence Model and Autonomy Allocation Function α

Using the data collected from the data collection process, we analyzed the robot performance based on PIJ and POT to identify a confidence model. The curve fitting toolbox in MATLAB [32] was utilized and multiple curves were fitted to the collected data with x = PIJ, y = POT, and c_a = HM (i.e. the confidence in the autonomous control in placing a suture in the right location). We examined first order to third order combinations of x and y and eventually variables x–y, x, and x^2 were chosen for candidate inputs to the model fits of data because of their strong positive relationship to c_a (i.e. correlation coefficient $R > 0.6$). Fig. 5.b shows results of our best fitted model which describes the data behavior according to the following

$$c_a = a + \frac{b}{e^{-c(x-y-d))}} + gx + hx^2$$

with $a = 0.031$, $b = 0.518$, $c = 10.68$, $d = 1.033$, $g = 0.032$, and $h = -0.0007$. According to Fig. 5.b, the fitted function suggests that the chance of the robot hitting a target suture point increases when the difference between PIJ and POT increases and vice versa. Similarly, more/less PIJ results in higher/lower chance of reaching a perfect suture location. The fitted curve in Fig. 5.b is defined as a confidence model for the robot (i.e. autonomous mode) performance.

An autonomy allocation function α can be determined once the confidence model is defined. The autonomy allocation function serves as a switch to indicate if a task is autonomous ($\alpha = 0$), or manual/assisted ($\alpha = 1$) based on the confidence model and a decision threshold τ. In an actual suturing task, an estimated HM chance of a planned suture point can be derived by mapping its PIJ and POT onto the confidence model. If the estimated HM lies beyond the threshold, the autonomy allocation function considers the robot is confident to accomplish the task autonomously ($\alpha = 0$ when $c_a \geq \tau$). On the other hand, if the estimated HM falls under the confidence threshold, the autonomy allocation function believes the robot needs supervision when performing tasks ($\alpha = 1$).

In the study, we choose two thresholds $\tau_1 = 0.854$, $\tau_2 = 0.9$ for our system to perform vaginal cuff closure in our experiments. The first threshold $\tau_1 = 0.854$ was chosen after performing pure autonomous targeting tests on vaginal cuff phantom with different open and close samples under rotated configurations (0°, 15°, and −15°) w.r.t. the z-axis shown in Fig. 4.g, evaluating how many target points were successfully reached. In the test, 41 target points were hit out of total 48. Thus, the success rate 0.854 (85.4%) was chosen as the

first decision threshold. The second decision threshold τ_2 was selected through confidence model in Fig. 5.b. To maximize robot performance in terms of accuracy, we selected τ_2 = 0.9 to be the decision threshold in the figure (i.e. success rate of 90% or higher as a decision threshold). We expect that the allocation function with a 90% threshold will be more conservative and will assign more tasks to the operator for supervising autonomous mode. The decision thresholds τ_1 and τ_2 were used in the final experiments.

C. Results of Vaginal Cuff Closure

Four robotic suturing experiments were conducted using STAR with our proposed method. STAR performed two suturing tasks for each decision threshold τ_1 and τ_2. Each task included completing a knot at the beginning followed by 11 running stitches and autonomous tensioning. We first compare the suturing results done by STAR and by manual method [24]. The results of the robotic and manual suturing are summarized in Table I with representative results shown in Fig. 6. The cuff closure using robotic technique in Fig. 6.a opened up slightly since no knot was placed at the end of the suturing task and the suture tension decreased after sample removal. In Table I, the task completion time for STAR is on average 10.8 minutes (647 seconds) longer and is on average 69.4 seconds slower in completing a stitch than the surgeon. Regarding the suture spacing and bite size, variance of both modalities are statistically less for STAR compared to that of the manual results ($p < 0.05$), which indicates STAR can place the running stitches more uniformly (1.6 times better) and is more consistent in bite depth (1.8 times better) compared to the surgeon.

From the results in Table II, it can be seen that the less conservative decision threshold τ_1 = 85.4% resulted in higher number of autonomous suture placement compared to τ_2 = 90% (i.e. 117% more considering total suggestions of 13 vs 6). However, τ_2 resulted in 100% successful hits compared to the 92.31% hit rate via τ_1, both of which were greater than the chosen thresholds. For the total of 19 predicted autonomous sutures, the prediction accuracy was 94.74% (i.e. 18 correct out of 19 guesses). The missed stitch occurred at the 11^{th} suture of the test which is very close to the final steps of the suturing process when the target tissue is almost closed and generally with a higher risk of missing an autonomous suture. This can be verified via the plots in Fig. 7 that show how the average predicted confidence in autonomous suture placement degrades closer to the end of the suturing task during the 4 tests. A representative example is shown in Fig. 6.c and Fig. 6.d, which can differentiate the easy and difficult parts of the suturing via the generally higher and lower number of green suturing points (i.e. the points that robot is confident in performing an autonomous suture placement). In these experiments 45.16% of the manual/assisted control suggestions happened in the first half of the suturing task (generally easier since the tissue is more open and approachable by the robot) and 54.84% in the second half (i.e. ratio of 0.82).

From the total of 33 sutures predicted in the manual/assisted mode, which warned the operator about the possibility of missing a stitch in the correct location, 12 stitches really required human intervention (i.e. 36.36% of the suggested stitches). This happens because we selected relatively high confidence levels for the decision threshold to guarantee a higher accuracy. Furthermore, based on the initial data collection and confidence model-fitting, we know that a miss is guaranteed only for suture points with very low confidence levels in the

autonomous mode. Therefore, these conservative predictions still provide valuable feedback for alerting the operator in the assisted mode to supervise the robot for possible misses and a need for tool-tip position corrections. In these tests, for each suture that required operator assistance, an average Euclidean distance of 3.99 ± 1.02mm w.r.t. its targeting location was added via the GUI to ensure the suture was placed in the correct location. For the total of 52 stitches placed using the confidence-based method, a total of 25% required human intervention (i.e. 12 missed stitches from the predicted assisted sutures and 1 miss from the predicted autonomous sutures).

IV. Discussion

The new confidence-based method takes a more conservative approach toward autonomous suture placement and hence increases the accuracy of autonomous suture placements from 85.4% in a pure autonomous suturing process to 94.74%. For the overall 52 suture placement attempts during the 4 tests, this accuracy is 98.1% by taking advantage of a 25% overall human intervention. However, this rate of intervention is considerably smaller compared to the case where a human needs to manually adjust all the sutures via the same robotic system without any use of autonomy.

Although the initial results from the proposed confidence-based strategy are promising, this method can further benefit from additional confidence measures such as the accuracy of the system calibration, non-uniform weighting for the PIJ and POJ points based on distance to the tool center, proximity of NIR markers and consecutive suture points, which may further improve the accuracy of the predictions. Moreover, a 3D camera with a higher resolution can significantly improve the accuracy of point cloud based estimations.

V. Conclusion

We presented a novel supervised autonomous suturing method that enables STAR to perform confidence-based suturing task collaboratively with operators. Specifically, a confidence model as well as an allocation function were identified based on the point cloud information of the tool-tip. STAR performs autonomous suturing with our proposed method to predict whether it is confident to place a stitch successfully on a suture point or needs a positioning adjustment from the operator. The results demonstrate that with using the proposed confidence model, STAR can predict the success of pure autonomous fairly accurately as well as improve suture placement accuracy over pure autonomous control. Moreover, STAR achieves results with better consistency in suture spacing and bite size compared to the manual laparoscopic surgery. Future work will include additional confidence models and investigating dynamic thresholds to improve prediction accuracy for other suturing tasks, using a better 3D camera system to improve point cloud resolution, and improving the speed of the suturing procedures.

Acknowledgments

Research reported in this paper was supported by National Institute of Biomedical Imaging and Bioengineering of the National Institutes of Health under award numbers 1R01EB020610, and R21EB024707. The content is solely the responsibility of the authors and does not necessarily represent the official views of the National Institutes of Health.

References

[1]. Mercante G, Ruscito P, Pellini R, Cristalli G, and Spriano G, "Transoral robotic surgery (TORS) for tongue base tumours," Acta otorhinolaryngologica italica, vol. 33, no. 4, p. 230, 2013. [PubMed: 24043909]

[2]. Kang CM, Chi HS, Kim JY, Choi GH, Kim KS, Choi JS, Lee WJ, and Kim BR, "A case of robot-assisted excision of choledochal cyst, hepaticojejunostomy, and extracorporeal Rouxen-y anastomosis using the da Vinci surgical system," Surgical Laparoscopy, Endoscopy & Percutaneous Techniques, vol. 17, no. 6, pp. 538–541, 12. 2007.

[3]. Lum MJH, Friedman DCW, Sankaranarayanan G, King H, Fodero K, Leuschke R, Hannaford B, Rosen J, and Sinanan MN, "The RAVEN: Design and Validation of a Telesurgery System," The Int. J. of Robotics Research, vol. 28, no. 9, pp. 1183–1197, 9. 2009.

[4]. Moustris GP, Hiridis SC, Deliparaschos KM, and Konstantinidis KM, "Evolution of autonomous and semi-autonomous robotic surgical systems: a review of the literature," The Int. J. of Medical Robotics and Computer Assisted Surgery, vol. 7, no. 4, pp. 375–392.

[5]. Kazanzides P, Mittelstadt B, Musits B, Bargar W, Zuhars J, Williamson B, Cain P, and Carbone E, "An integrated system for cementless hip replacement," IEEE Engineering in Medicine and Biology Magazine, vol. 14, no. 3, pp. 307–313, 5 1995.

[6]. Hagag B, Abovitz R, Kang H, Schmitz B, and Conditt M, "RIO: Robotic-Arm Interactive Orthopedic System MAKOplasty: User Interactive Haptic Orthopedic Robotics," in Surgical Robotics. Springer US, 2011, pp. 219–246.

[7]. Knoll A, Mayer H, Staub C, and Bauernschmitt R, "Selective automation and skill transfer in medical robotics: a demonstration on surgical knot-tying," The Int. J. of medical robotics + computer assisted surgery: MRCAS, vol. 8, no. 4, pp. 384–397, 12. 2012.

[8]. Iyer S, Looi T, and Drake J, "A single arm, single camera system for automated suturing," in 2013 IEEE International Conference on Robotics and Automation (ICRA), 5 2013, pp. 239–244.

[9]. Li Y, Richter F, Lu J, Funk EK, Orosco RK, Zhu J, and Yip MC, "Super: A surgical perception framework for endoscopic tissue manipulation with surgical robotics," IEEE Robotics and Automation Letters, vol. 5, no. 2, pp. 2294–2301, 2020.

[10]. Kang H and Wen J, "Robotic assistants aid surgeons during minimally invasive procedures," IEEE Engineering in Medicine and Biology Magazine, vol. 20, no. 1, pp. 94–104, 1. 2001. [PubMed: 11211665]

[11]. Lu B, Chu HK, Huang KC, and Cheng L, "Vision-based surgical suture looping through trajectory planning for wound suturing," IEEE Transactions on Automation Science and Engineering, vol. 16, no. 2, pp. 542–556, 2019.

[12]. Pedram SA, Ferguson P, Ma J, Dutson E, and Rosen J, "Autonomous suturing via surgical robot: An algorithm for optimal selection of needle diameter, shape, and path," in 2017 IEEE International Conference on Robotics and Automation (ICRA), 2017, pp. 2391–2398.

[13]. Hwang M, Thananjeyan B, Paradis S, Seita D, Ichnowski J, Fer D, Low T, and Goldberg K, "Efficiently calibrating cable-driven surgical robots with rgbd fiducial sensing and recurrent neural networks," IEEE Robotics and Automation Letters, vol. 5, no. 4, pp. 5937–5944, 2020.

[14]. Tanwani AK, Sermanet P, Yan A, Anand R, Phielipp M, and Goldberg K, "Motion2vec: Semi-supervised representation learning from surgical videos," 2020 IEEE International Conference on Robotics and Automation (ICRA), 5 2020. [Online]. Available: 10.1109/ICRA40945.2020.9197324

[15]. Chipalkatty R, Droge G, and Egerstedt MB, "Less is more: Mixed-initiative model-predictive control with human inputs," IEEE Trans. on Robotics, vol. 29, no. 3, pp. 695–703, 2013.

[16]. Loizou SG and Kumar V, "Mixed initiative control of autonomous vehicles," in Proceedings 2007 IEEE Int. Conf. on Robotics and Automation. IEEE, 2007, pp. 1431–1436.

[17]. Dragan AD and Srinivasa SS, "A policy-blending formalism for shared control," The Int. J. of Robotics Research, vol. 32, no. 7, pp. 790–805, 2013.

[18]. Saeidi H, Wagner JR, and Wang Y, "A mixed-initiative haptic teleoperation strategy for mobile robotic systems based on bidirectional computational trust analysis," IEEE Transactions on Robotics, vol. 33, no. 6, pp. 1500–1507, 2017-12.

[19]. Kang H and Wen JT, "Autonomous suturing using minimally invasive surgical robots," in IEEE Int. Conf. on Control Applications. IEEE, 2000, pp. 742–747.

[20]. Selvaggio M, Abi-Farraj F, Pacchierotti C, Giordano PR, and Siciliano B, "Haptic-based shared-control methods for a dual-arm system," IEEE Robotics and Automation Letters, vol. 3, no. 4, pp. 4249–4256, 2018.

[21]. Song C, Ma X, Xia X, Chiu PWY, Chong CCN, and Li Z, "A robotic flexible endoscope with shared autonomy: A study of mockup cholecystectomy," Surgical Endoscopy, pp. 1–12, 2019.

[22]. Ma X, Wang P, Ye M, Chiu PWY, and Li Z, "Shared autonomy of a flexible manipulator in constrained endoluminal surgical tasks," IEEE Robotics and Automation Letters, vol. 4, no. 3, pp. 3106–3112, 2019.

[23]. Saeidi H, Opfermann JD, Kam M, Raghunathan S, Léonard S, and Krieger A, "A confidence-based shared control strategy for the smart tissue autonomous robot (star)," in 2018 IEEE/RSJ International Conference on Intelligent Robots and Systems (IROS). IEEE, 2018, pp. 1268–1275.

[24]. Kam M, Saeidi H, Wei S, Opfermann JD, Léonard S, Hsieh M, Kang JU, and Krieger A, "Semi-autonomous robotic anastomoses of vaginal cuffs using marker enhanced 3d imaging and path planning," in International Conference on Medical Image Computing and Computer-Assisted Intervention. Springer, 2019, pp. 65–73.

[25]. Leonard S, Wu KL, Kim Y, Krieger A, and Kim PCW, "Smart tissue anastomosis robot (star): A vision-guided robotics system for laparoscopic suturing," IEEE Transactions on Biomedical Engineering, vol. 61, no. 4, pp. 1305–1317, 2014. [PubMed: 24658254]

[26]. Le HND, Opfermann JD, Kam M, Raghunathan S, Saeidi H, Leonard S, Kang JU, and Krieger A, "Semi-autonomous laparoscopic robotic electro-surgery with a novel 3d endoscope," in 2018 IEEE International Conference on Robotics and Automation (ICRA), 2018 pp. 6637–6644.

[27]. Decker RS, Shademan A, Opfermann JD, Leonard S, Kim PCW, and Krieger A, "Biocompatible near-infrared three-dimensional tracking system," IEEE Transactions on Biomedical Engineering, vol. 64, no. 3, pp. 549–556, 2017. [PubMed: 28129145]

[28]. Ge J, Opfermann J, Saeidi H, Krieger A, and Joshi A, "Chronic in vivo study of a novel biocompatible marker for transoral robotic surgery," in Triological Society 123rd Annual Meeting at COSM Virtual Poster Session, 5 2020.

[29]. Millbourn D, Cengiz Y, and Israelsson LA, "Effect of stitch length on wound complications after closure of midline incisions: a randomized controlled trial," Archives of Surgery, vol. 144, no. 11, pp. 1056–1059, 2009. [PubMed: 19917943]

[30]. Saeidi H, Le HN, Opfermann JD, Léonard S, Kim A, Hsieh M, Kang JU, and Krieger A, "Autonomous laparoscopic robotic suturing with a novel actuated suturing tool and 3d endoscope," in 2019 International Conference on Robotics and Automation (ICRA). IEEE, 2019 pp. 1541–1547.

[31]. Rusu RB and Cousins S, "3d is here: Point cloud library (pcl)," in 2011 IEEE International Conference on Robotics and Automation, 2011, pp. 1–4.

[32]. "Matlab curve fitting toolbox." [Online]. Available: https://www.mathworks.com/products/curvefitting.html

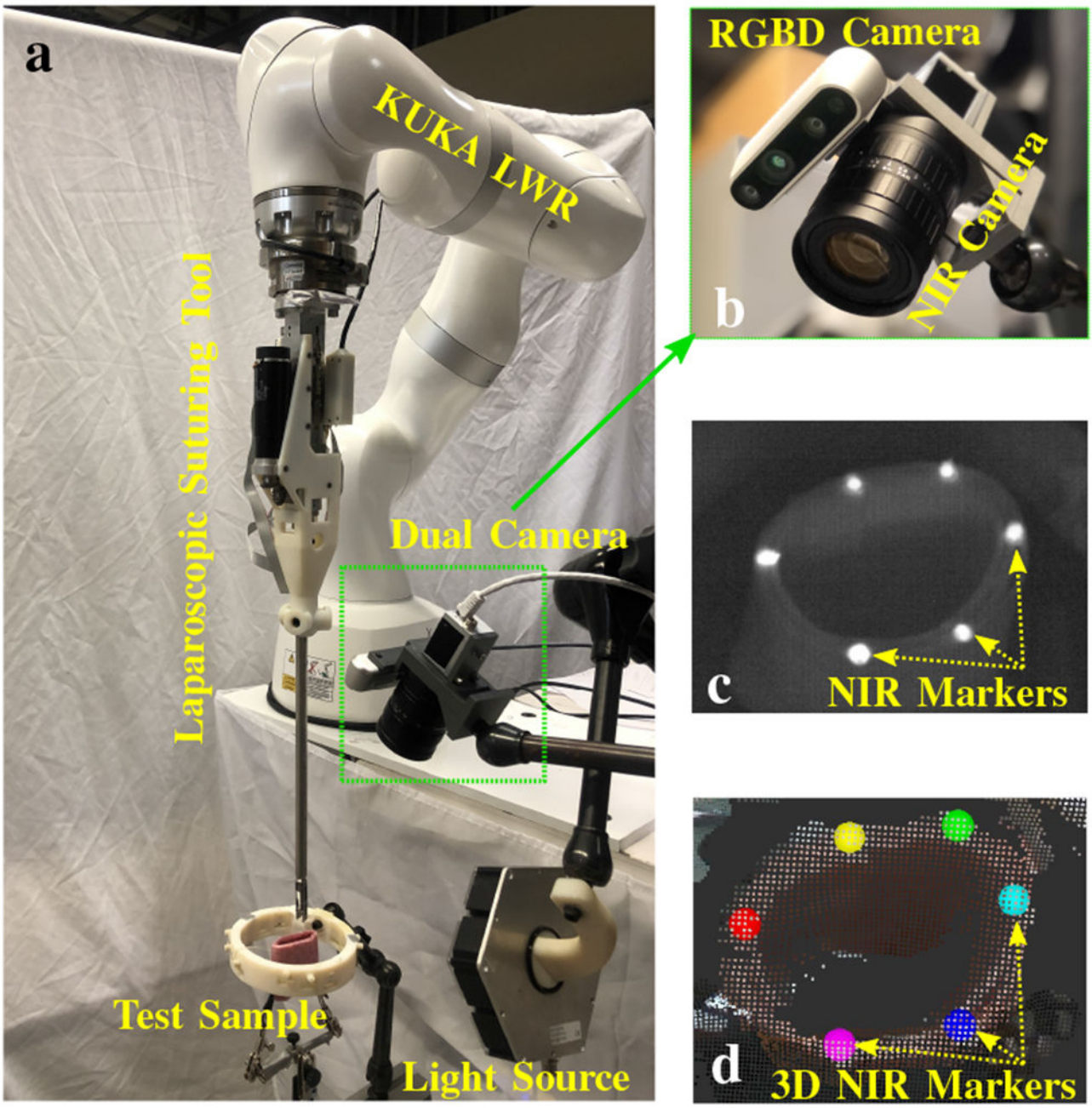

Fig. 1:

a) Experiment setup for confidence-based supervised autonomous vaginal cuff closure, b) dual camera system, c) NIR image view with NIR markers on the vaginal cuff phantom, and d) point cloud view from RGBD camera with 3D NIR marker overlaid.

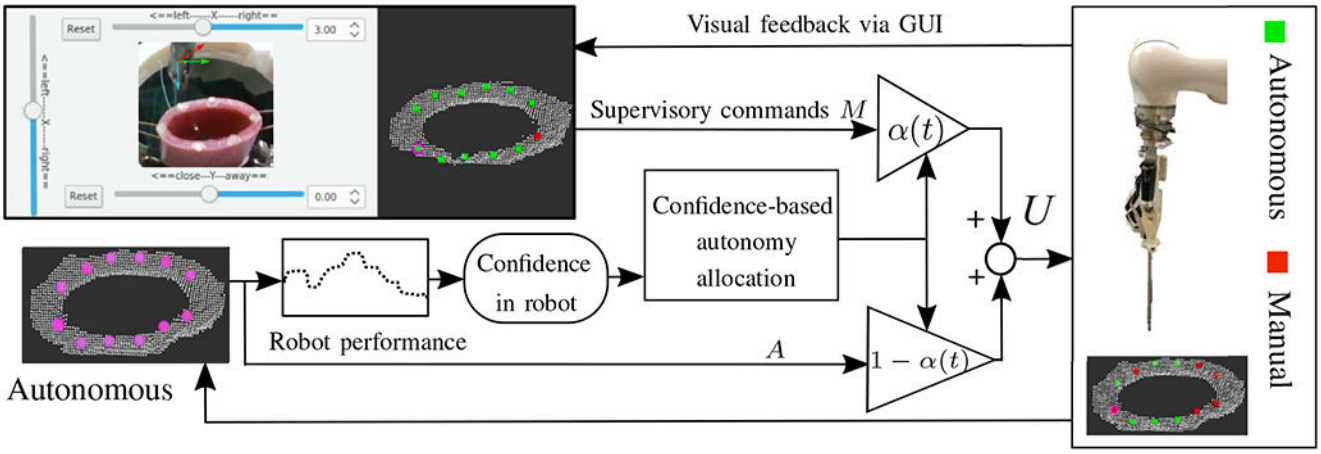

Fig. 2:
Conceptual block diagram of proposed confidence-based supervised autonomous suturing method.

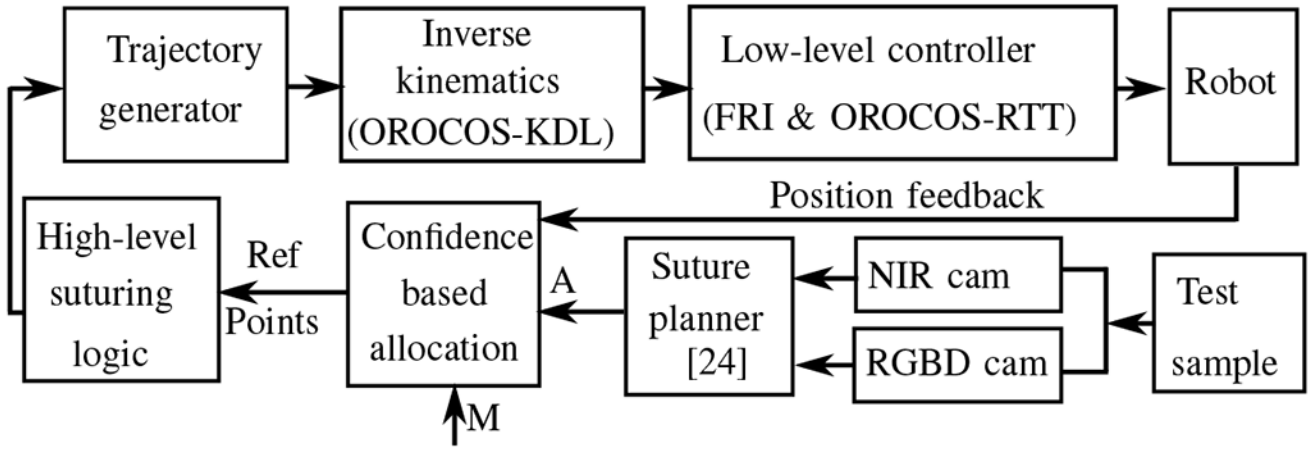

Fig. 3:
The autonomous control loop with confidence-based manual adjustments.

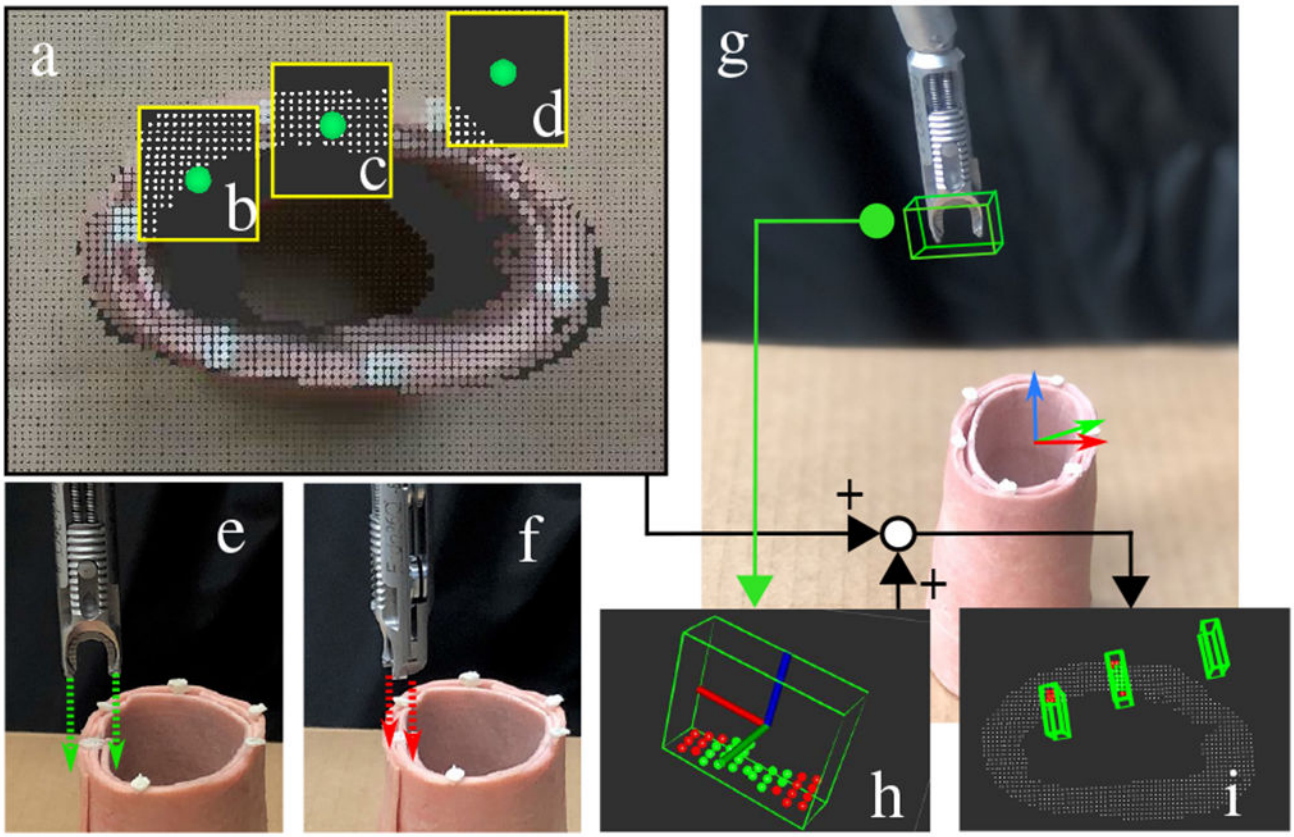

Fig. 4:

Examples of reaching suture points on a phantom vaginal cuff and steps of the data collection: a) Point cloud view with three suture points selected, b) a suture point is on an edge, c) a suture point has a high chance to be caught, d) a suture point has no chance to be caught, e) a good orientation of a tool-tip to reach suture points, f) a bad orientation of the tool-tip to reach suture points, g) rectangular box model of tool-tip, h) the projected rectangular box containing two groups of point cloud, and j) projected rectangular boxes to collect data on multiple suture points.

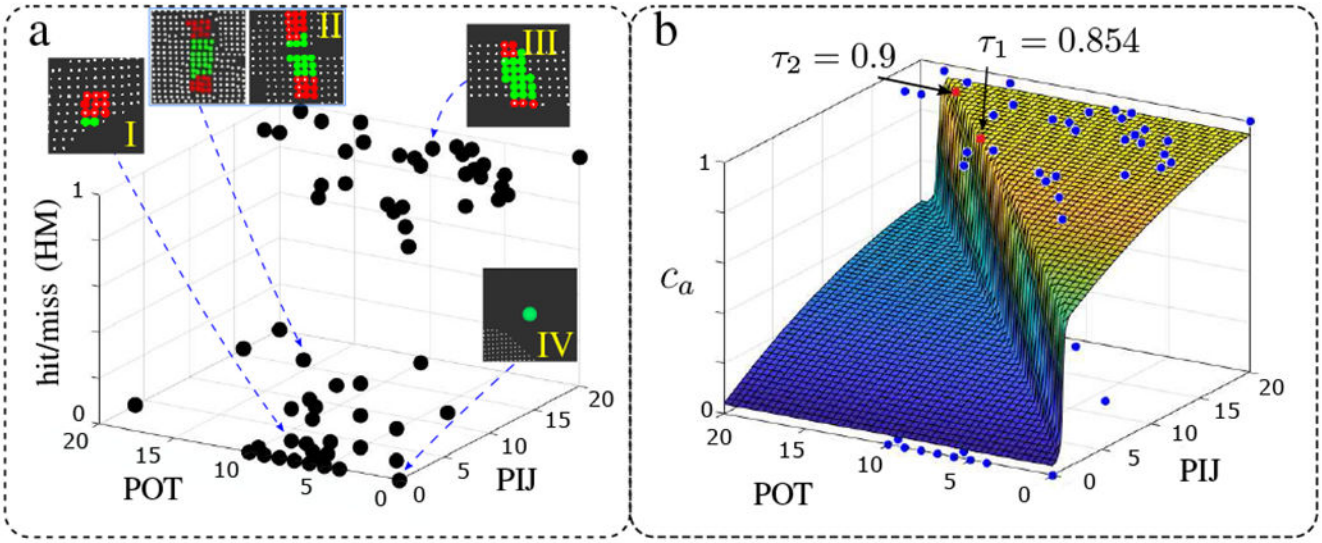

Fig. 5:

Result of data collection and confidence model identification. Data point examples of a.I) high POT but low PIJ, a.II) high POT and high PIJ, a.III) low POT but high PIJ, and a.IV) no POT and no PIJ. b) The confidence model identified for the confidence in autonomous (c_a) based on collected data.

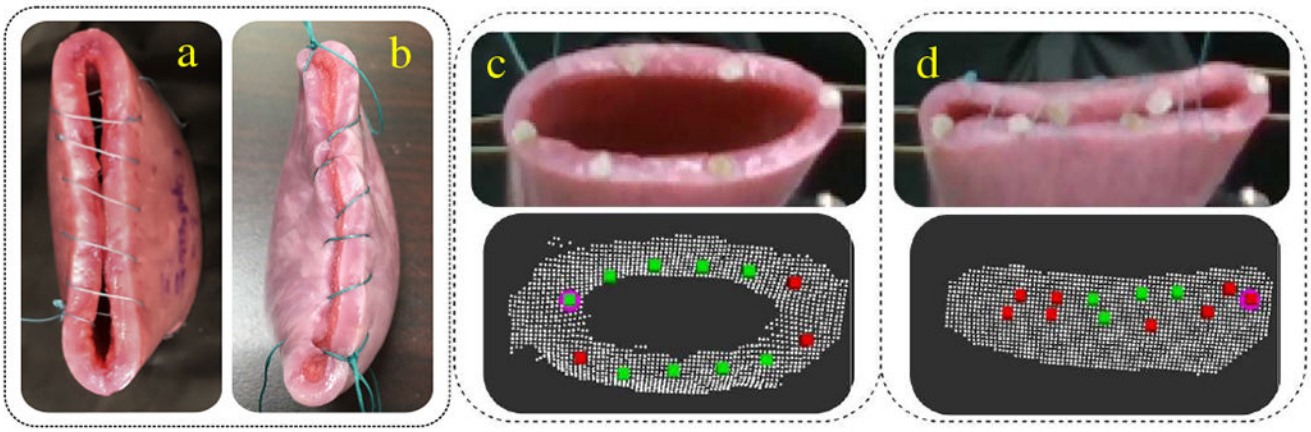

Fig. 6:

Results of synthetic vaginal cuff closure. a) STAR, and b) manual [24]. c) Higher number of green suture points before suturing. d) Lower number of green suture points after the vaginal cuff is closed.

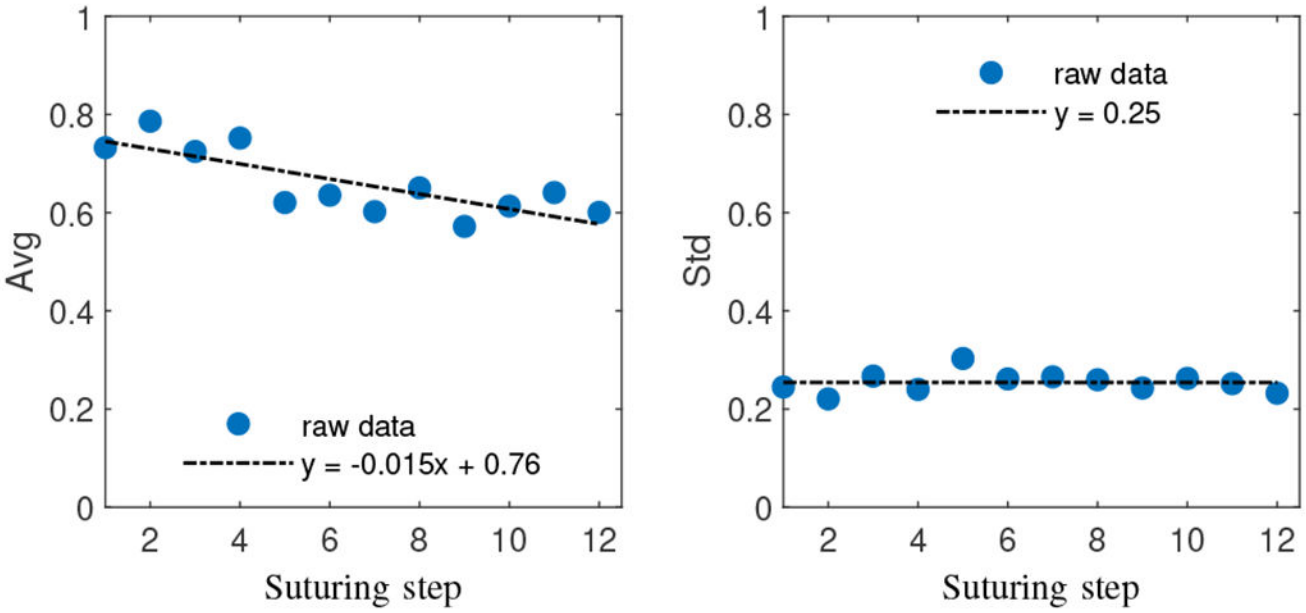

Fig. 7:
Average and standard deviation of confidence in autonomous suturing versus task progressions.

TABLE I:

Comparison of robotic and manual results.

Modality	Total time (min)	Time per stitch (sec)	Suture spacing (mm)	Bite size (mm)
STAR	17.7 ± 0.7	88.9 ± 23.2	7.41 ± 1.33	5.71 ± 1.34
Manual [24]	6.9 ± 0.2	19.5 ± 3.8	9.19 ± 2.08	4.96 ± 2.39

TABLE II:

Comparison of first attempt hit and misses based on the decision threshold (τ_1 = 85.4% and τ_2 = 90.% confidence levels) for a total 52 suture placements.

	Predicted/Suggested Mode					
	Auto			**Assisted**		
	***τ*1**	***τ*2**	**all**	***τ*1**	***τ*2**	**all**
Hit	12	6	18	10	11	21
Miss	1	0	1	3	9	12
Total	13	6	19	13	20	33